ACS APPLIED ENGINEERING MATERIALS

pubs.acs.org/acsaenm Article

Design and Fabrication of Polyisocyanurate Foams toward Significantly Enhanced Thermal Resistivity

Shiwanka V. Wanasinghe, Zoriana Demchuk, Achutha Tamraparni, Janak Tiwari, Tianli Feng, Catalin P. Gainaru, Bo Kyung Park, Sungjin Kim, Diana Hun, Tomonori Saito, and Som S Shrestha*

Cite This: ACS Appl. Eng. Mater. 2025, 3, 2087−2098

Read Online

ACCESS | Metrics & More | Article Recommendations

ABSTRACT: Developing high-performance thermal insulation is vital for addressing the ongoing global demand for reduced energy costs. Polyisocyanurate (PIR) foams are commonly used in residential and commercial buildings and in various industrial applications owing to their relatively high thermal insulation properties and fire resistivity. This study aims to further improve the thermal resistivity of PIR foams by (1) incorporating low thermal conductivity blowing agents; (2) tailoring the anisotropy of their cells; (3) tuning polymeric isocyanate quantities; and (4) incorporating a facer barrier, while using steps that easily integrate into current manufacturing processes for PIR foams. The resulting PIR foams exhibit a significant enhancement in thermal resistivity, achieving initial values as high as 8.3 h·ft^2·°F/Btu/in., commonly abbreviated as R-8.3/in., which is a 20% improvement compared with that of commercially used PIR foams that achieve approximately R-7/in. The detailed analysis of thermal conductivity measurements, mechanical testing, and morphological characterization elucidates the structure−property relationships. The developed high-performance PIR foams provide a critical pillar for next-generation high-performance insulation, offering promising thermal insulation for buildings and many other applications that have a significant effect on global energy costs.

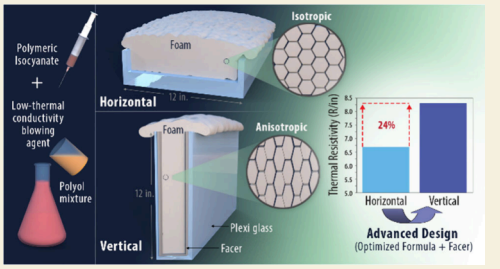

KEYWORDS: *Thermal insulation, Polyisocyanurate foams, Thermal resistivity, Anisotropic pores, Heat transfer*

1. INTRODUCTION

High-performance thermal insulation materials play a pivotal role in reducing overall energy costs in various applications, including buildings,[1] transportation,[2] refrigerators,[3] and medical uses.[4] According to the US Energy Information Administration, space heating and cooling accounted for over 50% of a household's annual energy consumption in 2020.[5] One major cause of this high energy consumption is under insulated commercial and residential buildings. Proper thermal insulation is vital in efficient heating and cooling of buildings because it minimizes heat flux through building envelopes.[6,7] By minimizing heat transfer, high-performance insulation materials contribute to lower energy cost.[8] Effective insulation often results in substantial long-term energy cost savings, while enhancing indoor comfort.

The thermal behavior of a material pertains to its interactions with heat, encompassing its ability to conduct and store thermal energy. In the context of thermal insulation materials, the main goal is to minimize heat transfer, effectively reducing the flow of thermal energy to maintain temperature differences across boundaries. The amount of heat transferred per unit area and thickness over a unit of time is commonly expressed as thermal conductivity. In insulation materials, thermal conductivity generally increases with rising temperatures and decreases as temperatures fall, highlighting the temperature-dependent nature of heat transfer in these materials.[9] Heat transfer through an insulation material primarily happens via 3 major ways: radiation, convection, and conduction. Radiative heat transfer involves the transfer of energy from a hotter surface or object to a cooler one through electromagnetic waves, primarily in the form of infrared radiation.[10] Convection is the process of heat transfer that occurs between two bodies due to the bulk movement of fluids, which can be either gases or liquids.[11] Typically, convection becomes a significant mode of heat transfer in porous solids when the pore size exceeds approximately 10 mm under an atmospheric pressure (1 atm). In the case of pore sizes less than 4 mm, convection becomes negligible, effectively restricting air movement within the structure.[12,13] Conduction heat transfer involves the movement of energy carriers, such as phonons, molecules, and atoms, between materials in direct contact, driven by a temperature gradient. It occurs through two main pathways: solid conduction, which relies on lattice

Received: April 9, 2025
Revised: June 26, 2025
Accepted: July 1, 2025
Published: July 7, 2025

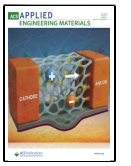

vibrations, and gas conduction, where heat transfer happens through collisions between neighboring gas molecules during random motion.[14] High-performance insulation materials exceed the limitations of gas conduction through the Knudsen effect by utilizing heavy gases, nanopores, or vacuum materials.[15] Heat transfer in porous thermal insulation materials is complex due to the combined effects of solid and gas conduction, which interact to determine the material's effective thermal conductivity. Commercially available insulation materials can be categorized into three groups: conventional, alternative, and advanced. Commonly used conventional insulation materials include expanded and extruded polystyrene,[16,17] polyurethane and PIR,[18] fiberglass,[19] and mineral wool.[20] For instance, expanded polystyrene, a widely utilized conventional thermal insulation material, exhibits thermal conductivity values (k) ranging from 0.031 to 0.037 $W{\cdot}m^{-1}{\cdot}K^{-1}$ (R-value per inch [R/in.] 3.9−4.65), respectively.[16,21] (Note: The R/in unit is $h{\cdot}ft^2{\cdot}°F/Btu$/in. [hour-feet squared degrees Fahrenheit per British thermal unit per inch].) Furthermore, hemp,[22] sheep wool[23] and jute fiber[24] are well-known alternative insulation materials. Advanced insulation materials include vacuum insulation panels,[25] and aerogels,[26] which exhibit exceptionally low thermal conductivity values along with low density. However, their high cost, uncertain long-term stability, low mechanical strengths, and/or inflexibility in terms of design and application have hindered the broader adoption of these advanced materials.[11]

PIR foam is a widely used conventional insulation material[27] known for its high thermal resistivity and durability.[28] The manufacturing process of PIR foam consists of a chemical reaction between a polyol and aromatic isocyanates in the presence of a blowing agent, where the isocyanate is taken in the excess. Tuning the isocyanate content in PIR foams is crucial because a higher content of isocyanate leads to the formation of more isocyanurate rings in the foam, which increases its rigidity and affects its material properties, including compressive strength, toughness, and thermal stability of the resulting foams. Therefore, hybrids of PIR and polyurethane (lower isocyanate content compared to PIR) are preferred because containing both types of material allows tuning of the hybrid's final mechanical performance.[29] Identifying the optimal ratio of polyol:isocyanate is crucial for developing insulation foam with enhanced performance. Current PIR-based foam boards in the market have initial thermal resistivity (R/in.) of 6.5−7.0 (i.e., k of 0.021−0.026 $W{\cdot}m^{-1}{\cdot}K^{-1}$), which needs to be further improved to reduce energy costs.[30] Various studies have explored factors that impact the thermal conductivity of rigid foams.[31−37] However, optimizing formulations is challenging because of trade-offs between various design parameters. For example, fiber reinforcement of PIR rigid foams by agricultural waste was found to enhance compressive strength but increase thermal conductivity.[35] Other formulation studies for rigid polyisocyanurate foams include optimizing metal and amine catalysts for isocyanurate generation,[38] or matrix type, reactant molar ratio, synthesis conditions, modifying agents along with catalysts.[39] Despite these optimizations, researchers still observed a limited R/in. of 4.9−5.7. (k = 0.0254−0.0294 $W{\cdot}m^{-1}{\cdot}K^{-1}$).[39] Furthermore, recent advancements in PIR foam technology have emphasized enhancing the initial thermal insulation performance while minimizing the aging of PIR foams. A significant innovation in this area is the adoption of hydrofluoroolefin (HFO) blowing agents, which present a lower thermal conductivity compared to traditional hydrofluorocarbon (HFC) alternatives. Torres-Regalado et al. demonstrated that varying the HFO content in PIR foams affects not only mechanical properties but also the aging behavior of the foams.[40] This research aimed at increasing the thermal resistivity of PIR foams to be beyond the state-of-the-art values of R-7/in. while matching the mechanical strength and material properties of commercial PIR foam insulation.

The present study explored an advanced approach for the fabrication of high-performance PIR foams based on modifying the cellular structure and tuning the formulation. Adjusting the formulation entails exploring the impact of water content, combination of blowing agents, and concentration of polymeric methylene diphenyl diisocyanate (pMDI). The cellular structure was tailored through the design of the mold that was used to fabricate the foams, which influenced the anisotropy of the cellular structure of the foams, enhanced the retention of the blowing agent, and reduced the level of heat transfer. In addition to the mold design, another approach to improve the thermal performance of PIR foam boards was by adding facers with low permeance on both sides of the foam to prevent the escape of blowing agents from the cells during foam formulation.[41,42] This design effectively preserves the low thermal conductivity gas composition within the foam, thereby minimizing the aging of its initial high R/in value, a significant challenge associated with the thermal conductivity of PIR foams. By using facer film with diffusion-tight bonding between the foam and facer, our approach helps prevent the diffusion of the blowing agent from the foam and the entry of high thermal conductivity atmospheric gases such as O_2, N_2, ultimately contributing to improved long-term thermal performance of novel PIR foams. A combination of these parameters significantly increased initial thermal resistivity, with an R-8.3/in., which is 20% higher than the initial thermal resistivity of current PIR foams on the market. This novel PIR foam is made by a highly adaptable and scalable fabrication process that uses readily available materials, providing a path for commercialization and deployment.

2. MATERIALS AND METHODS

2.1. Materials

All chemicals used in this study were provided by commercial suppliers and are given in Table 1. Two main components, polyol PS2352 and polymeric methylene diphenyl diisocyanate (pMDI), were provided by GAF Materials/Stepan Company and BASF, respectively. The polyurethane catalyst, blowing catalyst, and silicon surfactant (TEGOSTAB B8513) were supplied by Evonik Industries. The trimerization catalyst was provided by Milliken & Company. The fire-retardant agent tris(chloroisopropyl) phosphate (TCPP) was purchased from Ambeed, and blowing agents Opteon 1100 and 1150 were provided by The Chemours Company.

2.2. Methods

This section outlines a detailed description of the experimental design, material characterization, foam formulation, and procedure for foam synthesis.

2.2.1. Foam Preparation. *a. Using Horizontal Mold.* Polyol and the blowing agent were cooled to − 2 °C overnight before the reaction was initiated for all samples, unless otherwise specified in this paper. This precooling step provided additional time for the components to mix homogeneously before the chemical reaction began. Part B (Table 1) was mixed at 500 rpm for 3 min using an overhead mixer, followed by the addition of the blowing agent and further mixing at 500 rpm for 15 s. After pMDI was added, the mixture was stirred at 2,000 rpm for 10 s to ensure thorough blending

https://doi.org/10.1021/acsaenm.5c00263
ACS Appl. Eng. Mater. 2025, 3, 2087−2098

Table 1. Chemical Components Used to Make Polyisocyanurate Foams[a]

Component	Weight percentage (%)
Part A	
pMDI	40−70
Part B	
Polyol	30−60
Trimerization catalyst	0.5−0.8
Gel catalyst	0.1−0.3
Blowing catalyst	0.1−0.3
Surfactant	0.8−2.0
Fire retardant	3.0−4.5
Blowing agent	10−15
Deionized water	0.2−0.5

[a]The basic formulation for each component (A and B) is outlined in the table. Section 3 of this paper discusses optimization studies that explore varying quantities of water (0−0.2% w/w), different mixtures of blowing agents (Opteon 1100/Opteon 1150 at ratios of 100:80, 80:20, 50:50, 20:80, and 0:100), and changes in isocyanate concentration (42%, 48%, and 54% w/w).

of Parts A and B. The final mixture was then quickly transferred to a cardboard mold where expansion happened and allowed to cure for 24 h in the fume hood before the foam's thermal conductivity was assessed.

b. Using Vertical Mold. The mold is constructed using two pieces of plexiglass secured to a wooden frame. For samples requiring facer films, the plexiglass is covered with a facer film; otherwise, aluminum foil is used to prevent the foam from sticking on the plexiglass. The foam mixture, prepared according to the aforementioned steps in (a), is poured into the mold and allowed to cure for 24 h before testing for thermal conductivity.

2.2.2. Thermal Conductivity Measurements. Thermal conductivity was measured in the heat flow meter apparatus at 24 °C (75 °F), following the ASTM International (ASTM) C518 standard.[43] The sample size is 8−12 in. in width and length, with a thickness of 1 in. The densities of the foams were calculated by using the ratio of mass to volume. Two equilibrium criteria were used for the thermal conductivity measurements: (1) the average temperature of each HFM plate within the measurements must remain within ± 0.2 °C of the set point temperature, and (2) the difference in the average signals of the heat flux transducers between two successive measurements must be within 40 μV and 2%. In this work, data points for each sample were analyzed for an average of five measurements using HFM. Additionally, 2−3 replicates were used for specimen to calculate the error in measurement.

2.2.3. Scanning Electron Microscopy (SEM) Analysis. Samples were first cut into thin slices by using a sharp razor blade. The thin slices were then mounted onto SEM stubs by using double-sided carbon tape. The morphological characteristics of foams were analyzed using SEM (Hitachi S4800) at an accelerating voltage of 20 kV, with magnifications ranging from 30 to 800,000×. Two samples were tested to assess consistency, and the results demonstrated a similar outcome.

2.2.4. Gas Pycnometry. Gas pycnometry was conducted to analyze the open and closed cell fractions in the foam using micrometrics (Accupyc II 1340) following the ASTM D-6226-15 standard.[44] The sample size was 1 × 1 × 1 in. (25.4 × 25.4 × 25.4 mm). The samples were sealed in a 100 cm^3 instrument sample chamber, and the measurements were performed at room temperature by using nitrogen gas at an equilibration rate of 0.005 psig/min. Two replicates were performed by averaging over 10 measurement cycles, with a standard deviation of less than 2% of the measured values for all measurements.

2.2.5. Compressive Strength Experiment. The compressive strength experiment was conducted using an Instron machine equipped with a 1 kN load cell at a 2.5 mm/min strain rate until samples reached 13% deformation or yield, whichever occurred first. Three to five samples measuring 1 × 1 × 1 in. (0.08 × 0.08 × 0.08 ft) were tested to obtain the standard deviation.

2.2.6. Thermogravimetric Analysis (TGA). TGA measurements were performed using a TA Q550 under a nitrogen atmosphere. Foam samples of 1−5 mg were placed on TGA high-temperature platinum pans and measured using analytical balance. The samples were tested in the temperature ramp regime from 25 to 700 °C with a constant heating rate of 10 °C/min. A single run was conducted due to logistical constraints associated with the instrument.

2.2.7. Fourier-Transform Infrared (FTIR). FTIR spectra were acquired using a Bruker INVENIO R equipped with an attenuated total reflectance (ATR) accessory. The FTIR spectra were collected over the range of 4000 to 400 cm^{-1} with a resolution of 4 cm^{-1}, averaging 254 scans per sample at room temperature. Background spectra were subtracted from each sample spectrum to correct for atmospheric interference. Three replicates were conducted. The Solid + Gas and Radiation components were calculated using FTIR measurements, yielding a standard deviation of 0.06.

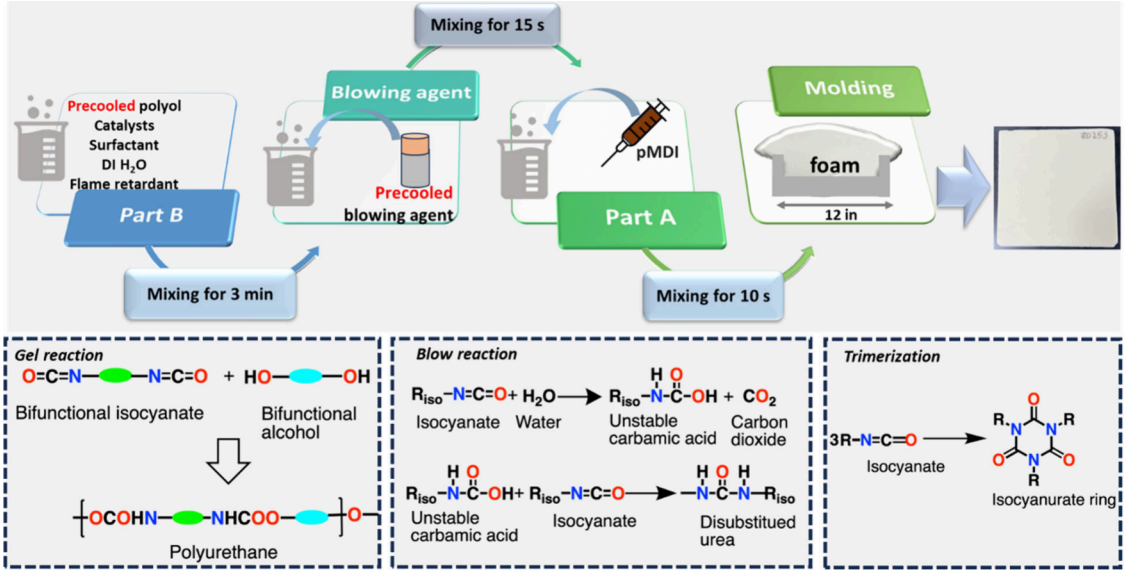

Figure 1. Schematic diagram of the synthesis of polyisocyanurate foams.

https://doi.org/10.1021/acsaenm.5c00263
ACS Appl. Eng. Mater. 2025, 3, 2087−2098

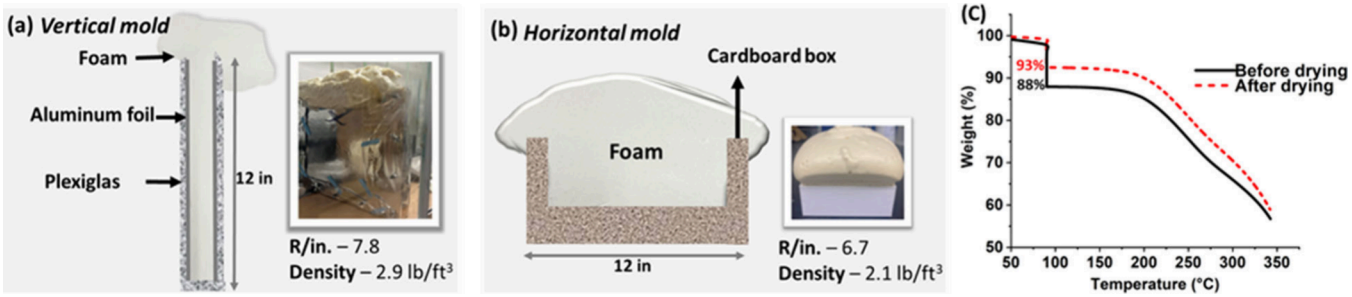

Figure 2. Effects of mold type: (a) The vertical mold, a wooden frame with Plexiglas sheets and aluminum foils attached on both sides, measures 12 × 12 × 1 in. (b) The horizontal mold is a cardboard box with one open side. (c) The isothermal TGA analysis on polyol before and after drying (sample is dried at 105 °C for 24 h) includes a temperature scan with a 5 h isothermal step at 90 °C in air and a heating rate of 10 °C/min.

2.2.8. Hydrophobic Test. Contact angle measurements were taken with the Attention Optical Tensiometer using the standard sessile drop function included with the machine's OneAttension software. The liquid used for this testing was distilled water. The droplets measured for contact angle testing are about 5 μL, or roughly the size of a 4 mm steel ball bearing. The sample is placed on the machine's loading surface to where it can be seen with the camera, and a red line is then dragged by the user to the sample's surface. The droplet is lowered to the sample's surface. Values are reported as the mean of triplicate experiments with a standard deviation of 7°.

3. RESULTS AND DISCUSSION

PIR foams were prepared by mixing two main components—Part A and Part B—in the presence of additives, as shown in Table 1 and Figure 1. Several reactions take place during the formation of polyurethane and PIR (Figure 1), and catalysts are necessary for these processes. This formulation was composed of three major catalysts: a trimerization catalyst, a blowing catalyst, and a gel catalyst. Surfactants were added to stabilize the foam, and a fire retardant (TCPP) was included to improve the fire resistance. The polyol was first mixed with the additives, followed by the addition of the blowing agent, after which pMDI was incorporated into the mixture. Two parts were mixed at a high rpm for a few seconds owing a uniform, high-quality PIR foam by ensuring efficient bubble formation, improved reaction kinetics, and a finer cellular structure (increased number of nucleating sites) (Figure 1).

Density is a crucial parameter that directly influences the thermal resistivity of the PIR foams. Lower-density foams are desirable because they have more porosity and consume fewer raw materials, making them more cost-effective compared to high-density foams. Adjusting the water content in the formulation is one way of tuning the density of foams. During initial optimization studies, drying polyol under vacuum overnight was found to considerably increase the R/in. value of the foams by 7%, which could be explained by the removal of excess bonded water and low-volatile compounds. This observation was further supported by TGA, as shown in Figure 2(c), which indicates a 5% reduction in water content after drying. Table 2 illustrates the thermal conductivities and densities of samples with different water contents (Samples A-C). To keep expansion at the same level, cyclopentane (thermal conductivity of approximately 11.6 mW·m^{-1}·K^{-1}) was used as a blowing agent (Sample D) to compensate for the removal of water from the formulation. In addition, a sample with a mixture of blowing agents (Sample E) that have similar thermal conductivities was synthesized to provide different blowing abilities. Opteon 1100 (33.4 °C [1 atm], thermal conductivity 10.4 mW·m^{-1}·K^{-1} at 20 °C) and Solstice liquid blowing agent (19 °C [1 atm], thermal conductivity 10.2 mW·m^{-1}·K^{-1} at 20 °C) have different boiling points. We assumed that the boiling points would influence the blowing abilities.

Table 2. Effects of Different Water and Blowing Agent Quantities on the Thermal Performance of the Polyisocyanurate Rigid Foam[a]

Parameter/Sample[b]	A	B	C	D*	E
Water content w/w (%)	—	0.1	0.2	—	0.2
Opteon 1100 w/w (%)	9.0	9.0	9.0	—	6.9
Solstice liquid blowing agent w/w (%)	—	—	—	—	2.2
Cyclopentane w/w (%)	—	—	—	9.0	—
R/in. value	**6.0**	**6.5**	**6.5**	**5.6**	**6.4**
Density (lb/ft³)	**3.3**	**2.6**	**2.4**	**1.7**	**2.3**

[a]Notes: sample dimensions are 8 × 8 × 1 in. (203 × 203 × 25.4 mm). Thermal conductivity was measured in the heat flow meter apparatus according to ASTM C518 standards. The polyol was placed under vacuum at 75 °C overnight. The R/in. value is determined based on the average of two samples with a difference of less than 4%. [b]w/w = weight per weight.

For the study of water content impact, samples prepared under identical conditions and using the same blowing agent were considered (samples A, B, and C). According to the results, the sample with 0.2% w/w of water (Sample C) exhibited the lowest density, showing a 27% reduction, and also demonstrated an 8% increase in the R/in. value compared with that of the control sample without water (Sample A). This improvement in R/in can be attributed to the enhanced expansion, confirmed by the corresponding decrease in density. In the initial nucleation process, water acts as a chemical blowing agent, reacting with isocyanate and producing CO_2. These results show that the foam density can be adjusted by modifying the water content while maintaining or even improving the R/in. value. In addition, the results demonstrated that the presence of cyclopentane considerably decreased the density by approximately 49% compared to the control sample (A); however, the R/in value also decreased by 7%, likely owing to the higher thermal conductivity of cyclopentane (Sample D). The notable reduction in the density of cyclopentane may be attributed to its lower solubility in the polyol used for foam preparation, especially when compared with the solubility characteristics between Solstice and polyol. Solubility is a critical parameter, as it is well established that the density of foams produced with cyclopentane significantly varies in accordance with the solubility index.[43] Foams with a mixture of blowing agents (Sample E) showed similar R/in. and densities compared with those of the samples with a single blowing agent (i.e., 100%

https://doi.org/10.1021/acsaenm.5c00263
ACS Appl. Eng. Mater. 2025, 3, 2087−2098

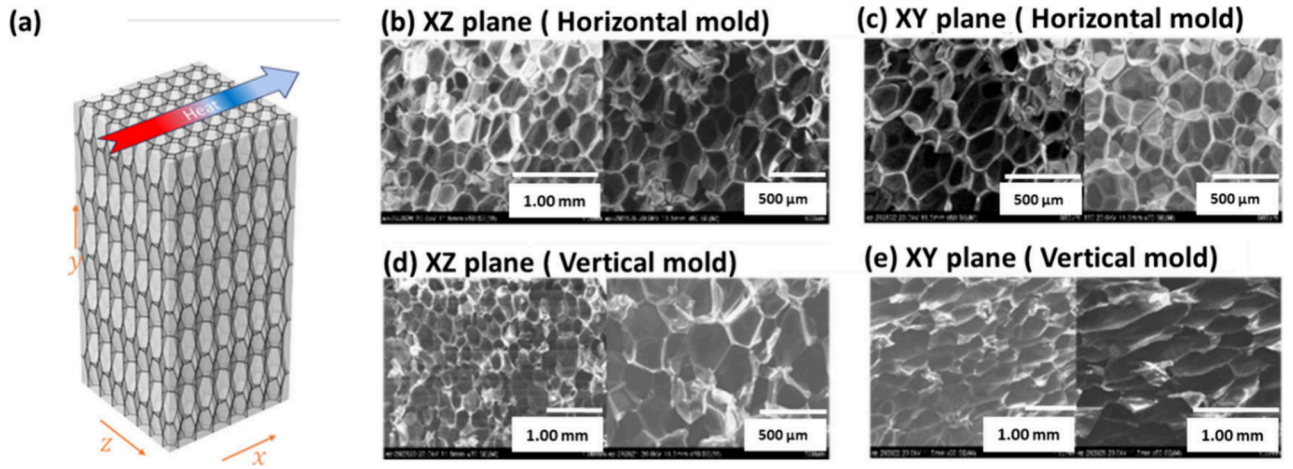

Figure 3. SEM images of the foam under study: (a) A pictorial representation of the foam for SEM analysis illustrates the direction of heat flow. SEM images show samples made with the horizontal mold along the (b) XZ and (c) XY planes and with the vertical mold along the (d) XZ and (e) XY planes.

Opteon 1100, Sample C). This could be attributed to the difference in boiling points between the two blowing agents being insufficient to significantly influence blowing capabilities. Therefore, the formulation with Opteon 1100 (Sample C) was chosen for further experiments to examine the effect of the mold design, which is discussed in the next section.

Preserving the blowing agent in the reaction mixture during foam fabrication is essential to achieve higher thermal resistivity. The mold type plays a significant role in retaining the blowing agent, because it serves as a physical barrier. To explore the influence of mold design in the thermal performance of PIR foams, samples were prepared using two distinct mold types: vertical and horizontal (Figures 2a and 2b). We hypothesized that because it has a smaller area exposed to ambient conditions, the vertical mold would be better than the horizontal mold in retaining the blowing agent. The results validated this hypothesis, showing a significant 16% improvement in the R/in of PIR foams prepared using the vertical mold yielding an R-7.8/in., whereas the PIR foams prepared using the horizontal mold showed an R-6.7/in. Replicate studies demonstrated the reproducibility of the findings, validating their consistency across different trials, with a difference of less than 0.5% compared to the listed R/in (sample size 2−3). Lower R/in. in horizontal mold samples suggests that during the exothermic reaction, a larger proportion of the blowing agent might escape through the horizontal mold, which has a wider space for the foam to expand until reaching the gel point. In contrast, more restricted space in the vertical mold can retain a higher amount of blowing agent owing to the limited space for foam expansion until the gel point is reached. Consistent with the hypothesis, results showed that the density of foams produced using the vertical mold increased by approximately 40% (to 2.9 lb/ft^3) compared with that of the horizontal mold foams (2.1 lb/ft^3), which also rationalize the combined effects of restricted expansion and higher retention of the blowing agents within the foam. Moreover, gas pycnometry experiments were conducted to evaluate the closed cell content of the foam samples, offering a deeper understanding of their internal characteristics. Aligned with the thermal insulation performance, vertical molded samples showed a slightly higher closed cell content (89%) compared with that of foams prepared using a horizontal mold (84%).

Moreover, the geometry of the mold can influence the cell structure, which may affect thermal pathways within the foam and its thermal resistance. To investigate this effect, we performed SEM analysis on samples prepared by using both horizontal and vertical molds. The foam structure used in the SEM analysis is depicted in Figure 3a, with the direction of heat flow indicated by an arrow. By sectioning the foam along the XZ and XY planes, we analyzed pore structures along and perpendicular to the direction of heat transfer. For the foam prepared by using the horizontal mold, the pore size along all three axes is nearly equal, as shown in Figures 3b and 3c, indicating that the foam prepared by using a horizontal mold is nearly isotropic. In contrast, the foam prepared with the vertical mold, *Pore size* $(D)D_y \gg D_x$ (see Figure 3e), while $D_y \approx D_x$ (see Figure 3d), exhibits prolate pore geometry with high anisotropy (anisotropic ratio of 3.8). The more confined geometry along the X and Y directions in the vertical mold, relative to the Z direction, explains the formation of the anisotropic pore geometry. This anisotropic pore geometry distorts the heat transfer path,[46] forcing heat flow to take longer and more tortuous paths, which reduces thermal conduction through the solid walls of porous foam. Our observations using SEM reveal that the elongated cells, which were prepared using a vertical mold, exhibit a high anisotropic ratio of 3.8. This pronounced anisotropy plays a crucial role in reducing solid thermal conductivity as it modifies the pathways through which heat can flow. The distortion of heat flow caused by the elongated cell structure creates barriers that impede the transfer of thermal energy, ultimately leading to a decrease in the overall thermal conductivity. The higher R-7.8/in. observed for the sample produced using the vertical mold, compared with R-6.7/in. for the sample produced using the horizontal mold, can be attributed to the combined effects of higher closed cell content and anisotropic pore geometry in the vertical mold. The enhanced R/in. prompted us to use the vertical mold for further studies.

In addition to their superior thermal insulation properties, anisotropic cellular insulating materials exhibit an enhanced mechanical performance along specific directions, thereby garnering significant attention in recent years. Mechanical

https://doi.org/10.1021/acsaenm.5c00263
ACS Appl. Eng. Mater. 2025, 3, 2087−2098

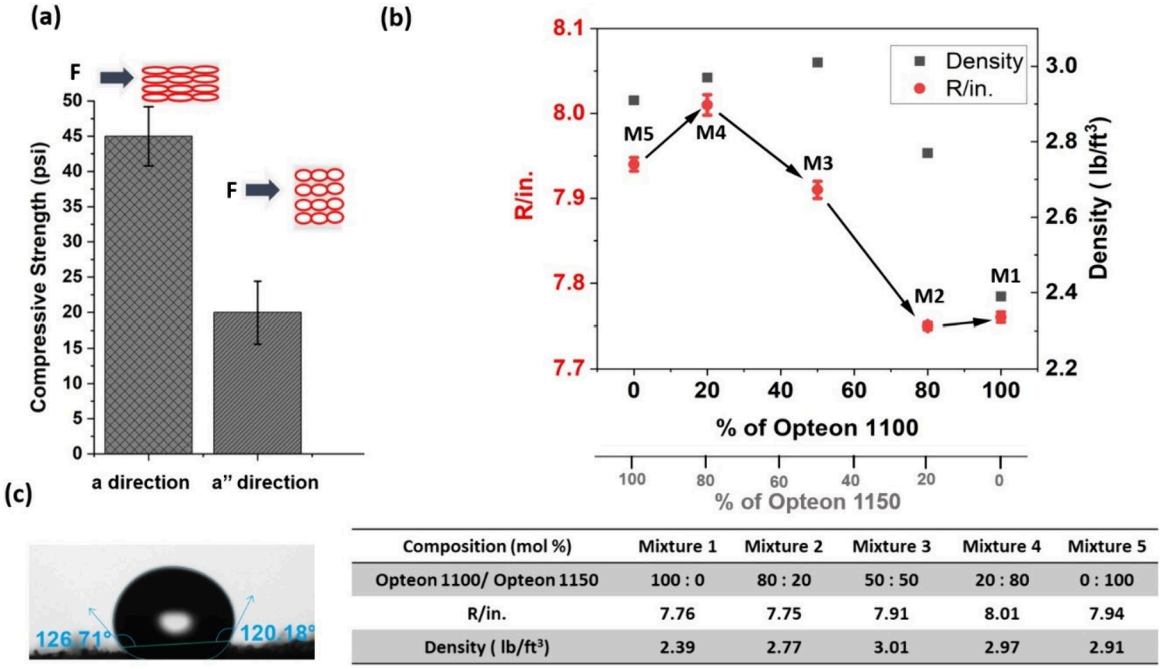

Composition (mol %)	Mixture 1	Mixture 2	Mixture 3	Mixture 4	Mixture 5
Opteon 1100/ Opteon 1150	100 : 0	80 : 20	50 : 50	20 : 80	0 : 100
R/in.	7.76	7.75	7.91	8.01	7.94
Density (lb/ft³)	2.39	2.77	3.01	2.97	2.91

Figure 4. (a) Effect of the anisotropic cells on the compressive strength of the foam samples. A total of three to five samples were tested and standard deviation is calculated. Foams prepared using vertical mold (a direction) and horizontal mold (a′′ direction); both a′ and a′′ directions are similar. (b) Effects of Opteon 1100 and Opteon 1150 on thermal performance and density. The standard deviation was calculated using the last five measurements of each individual replication. The error bars in the M1 and M2 are smaller than the marker size and are not clearly shown in the graph. (c) Hydrophobic test of PIR foam sample, with contact angle of 117 ± 7°. Six measurements were used to calculate the standard deviation.

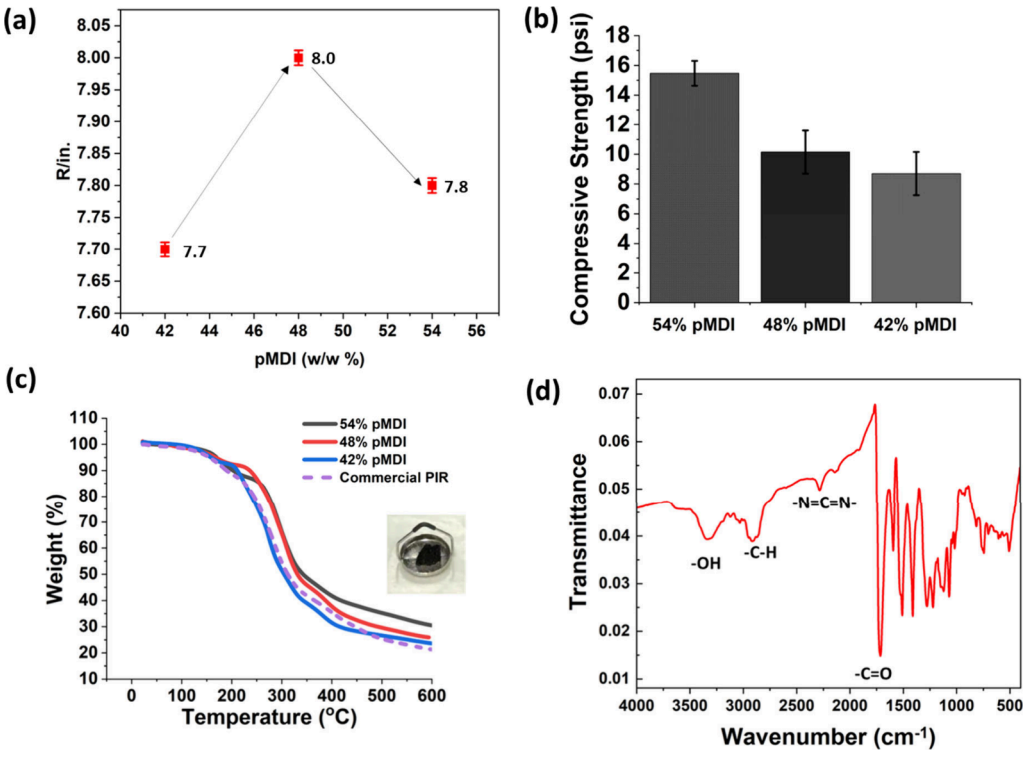

Figure 5. (a) Effect of pMDI content on thermal performance of polyisocyanurate foams with percentages calculated based on total mass of the formulation. Three replicates were utilized to calculate the standard deviation from the average of 15 measurements. (b) Compressive strength of foams with different pMDI percentages, three to five samples were tested, and the standard deviation is calculated. (c) TGA analysis of foams with different pMDI contents defined in Figure 5(a). (d) FTIR spectra of sample containing 48% w/w pMDI.

properties of different anisotropic insulating structures have been extensively reported in the literature,[47−54] consistently demonstrating significantly higher compressive strength along the anisotropic axis ([a] axis) compared with that along the transverse direction. Consistent with these findings, this study showed that the compressive strength of the PIR foams

https://doi.org/10.1021/acsaenm.5c00263
ACS Appl. Eng. Mater. 2025, 3, 2087−2098

prepared by using the vertical mold (anisotropic pore geometry) was strongly affected by the cell structure compared with that of foams prepared with the horizontal mold (nearly isotropic pore geometry). As shown in Figure 4a, vertically molded samples exhibited a 125% increase in compressive strength compared to the foams prepared using the horizontal mold (nearly isotropic foam) in [a] direction.

To further optimize the thermal insulation performance of PIR foams, we introduced Opteon 1150, which has an exceptionally low boiling point (7.5 °C) that is below room temperature. Because Opteon 1150 has a boiling point significantly lower than that of Opteon 1100 (33 °C), we assumed that the addition of Opteon 1150 would change the foam-blowing ability. Thermal resistivities and densities are shown in Figure 4b.

As shown in Figure 4b, the R/in. value remains largely unchanged between Mixture 1 and Mixture 2, indicating that the ratio remained consistently stable for both mixtures despite variations in the composition. However, a 15% increase in density was observed in the presence of 20% (w/w) Opteon 1150 in Mixture 2 compared with the density of Mixture 1 without Opteon 1150. This change in density confirms that the expansion ability changed when the blend composition was modified. Further addition of Opteon 1150 to the mixtures increased the R/in value by 2% in Mixture 3 over that of Mixture 2. However, the R/in. value remained stable with a variation of less than 2% among Mixtures 3, 4, and 5. This could be due to the optimum boiling point reached by the mixture, which appears to affect the blowing capacity of the foam. Moreover, Mixture 5 with 100% Opteon 1150 showed an R/in value relatively similar to that of Mixture 4. The similar R/in. values could be attributed to the relatively low boiling point of the Opteon 1150 alone affecting the overall behavior of the system and causing Opteon 1150 to rapidly escape from the foam during the exothermic reaction. Although Mixture 1 did not show the highest R/in, it was chosen for further studies because of its significantly lower density compared with that of the other mixtures. Figure 4c presents the results of the hydrophobicity test conducted on foam produced from mixture 1, which exhibited a contact angle of 117 ± 7°. This indicates that the samples are hydrophobic, meaning that they repel water. In the experiment, water droplets were placed onto the foam surfaces using a syringe, and the droplets were observed laterally under a microscope. The contact angle formed between the water droplet and the foam surface was measured to evaluate hydrophobicity: an angle greater than 90° indicates that the material is hydrophobic, while an angle less than 90° suggests that it is hydrophilic.[9] In addition, we have conducted tests on our material using Differential Scanning Calorimetry and determined the specific heat capacity at two different temperatures: 936 J/kg·K at 50 °C and 1308 J/kg·K at 100 °C.

The effect of the pMDI content on the thermal insulation performance of PIR foams was evaluated as shown in Figure 5a. The quantity of pMDI was reduced by 6% w/w (from 54% to 48%), resulting in a 3.4% improvement in the R/in. (from R/in. of 7.8. to R/in. of 8.0.). This improvement in thermal resistivity in the sample with 48% pMDI could be due to the lack of hard segments (mainly composed of isocyanurate rings) compared with the thermal resistivity of foams containing a higher proportion of hard segments, which form continuous heat channels that conduct heat more effectively. However, a further reduction of pMDI (42% pMDI) led to a 4% decrease in R/in., a change that could potentially have a significant effect on the secondary structure and closed cell content of the PIR foam that determines the thermal characteristics of the overall material. Replicate studies showed consistent results, indicating the reproducibility of all samples. To further validate the results, we analyzed the closed cell content of these compositions using pycnometry. Consistent with earlier findings, samples with 42% pMDI exhibited 52% closed cell content, representing a significant 29% reduction of closed cell content compared with samples containing 48% pMDI, which show 78% closed cell content. Both 54% and 48% pMDI offered less significant differences in closed cell content of 89% and 78%, respectively. Compressive strength of the foams was analyzed to investigate the effect of pMDI content on their mechanical properties. As expected, the corresponding results indicate that the pMDI content significantly affects the compressive strength of the foams (Figure 5b). Specifically, an increase in the pMDI content leads to higher compressive strength. This trend is consistent with the increased hard segment content in the foams, which is known to contribute to enhanced rigidity and strength.

Thermal stability of these foams was assessed through TGA experiments that measured the change in mass of a foam sample as the temperature was gradually increased.[55] The results indicated that foams remain stable up to approximately 200 °C (Figure 5c), beyond which decomposition begins. Char formation of the sample after TGA studies indicated the flame resistance of the material (Figure 5c). The char formation can function as a thermal shield, inhibiting the penetration of heat and oxygen that help to reduce flammability. The sample with 54% pMDI demonstrated a 31% char yield, whereas the samples with 48% and 42% pMDI showed char yields of 26% and 24%, respectively (Figure 5c). The commercial PIR foams exhibited the lowest char yield at 22%. Based on these findings, 48% pMDI was selected as the best formulation for further studies because of its promising R/in. FTIR analysis was carried out to confirm the presence of functional groups typically present in PIR foams.[33] The FTIR spectra show several characteristic absorption bands, including the polyurethane carbonyl (C═O) stretching vibration around 1710 cm^{-1}, the −N═C═N− stretching vibration near 2275 cm^{-1}, the hydroxyl (−OH) stretching vibration around 3300 cm^{-1}, and the C−H stretching vibration at approximately 2917 cm^{-1} as shown in Figure 5d.

To further improve the thermal performance of the high-performance foams, we introduced a low permeable multilayer facer film that serves as a physical barrier against water vapor and gas molecules such as O_2, CO_2, and N_2. The attached facer barrier will minimize outward diffusion of the blowing agent and inward diffusion of air. As a result, the addition of the facer barrier significantly improved the initial R/in. by approximately 4%, showing R/in. of 8.3 (sample size 2−3) compared with that of the control sample. Replication of the findings showed that the trials yielded similar outcomes. In addition to the initial R/in. values, facer barriers can play a significant role in reducing the thermal aging of PIR foams over time. Facer barriers minimize the diffusion of high thermal conductivity atmospheric gases and water vapor into the foam, while also preventing the escape of low thermal conductivity blowing agents. Ongoing tests are being conducted to evaluate the impact of these facer barriers on the long-term thermal performance of PIR foams, both with and without facers. Based on our ongoing tests, we have observed that PIR foams with

https://doi.org/10.1021/acsaenm.5c00263
ACS Appl. Eng. Mater. 2025, 3, 2087−2098

Table 3. R-Values/in., Total Thermal Conductivities, and Decomposed Contributions for Newly Developed High-Performance and Commercial Foams[a]

Foam	R/in.	Effective k_{eff} ($mW·m^{-1}·K^{-1}$)	Solid ($mW·m^{-1}·K^{-1}$)	Gas ($mW·m^{-1}·K^{-1}$)	Solid + Gas ($mW·m^{-1}·K^{-1}$)	Radiation ($mW·m^{-1}·K^{-1}$)
Commercial PIR (unaged)	7.0	20.6	3.9	15.1	19.0	1.6
Commercial PIR (aged)	5.5	26.2	3.9	20.7	24.6	1.6
High-performance foam (unaged)	8.0	18.0	—	—	15.2	2.8
High-performance foam (aged)	6.5	22.2	—	—	19.4	2.8
High-performance foam (unaged, with facer)	8.3	17.3	—	—	14.5	2.8
High-performance foam (unaged, if isotropic)	<6.7	>21.4	8.0	>10.6	>18.4	2.8

[a]The "—" indicates that solid and gas contributions could not be decomposed due to their coupled nature in the anisotropic foams. The standard deviation for both Solid + Gas and Radiation components in the high-performance foam is consistently 0.06 across all measurements.

facer barriers maintained a thermal resistance of up to R-7.4/in. after 180 days, while the foam samples without facer films exhibited a decrease to R-6.7/in. over the same period. These findings underscore the critical role of facer barriers in minimizing the effects of aging on thermal performance.

To compare the high-performance foams developed in the study with commercial foams, we decomposed the effective thermal conductivity (k_{eff}) from the gas, solid, and radiation using the modeling tool ThermoPI.[56,57] As shown in Table 3, the solid and radiation contributions in commercial PIR foams are about 3.9 and 1.6 $mW·m^{-1}·K^{-1}$, respectively. The gas contribution increased from 15.1 to 20.7 $mW·m^{-1}·K^{-1}$ after aging. The increase in thermal conductivity observed in commercial PIR foams may be attributed to low thermal conductivity blowing agents escaping out, while high thermal conductivity atmospheric gases and water vapor permeate into the foam, which causes the rise in thermal conductivity as time progresses. In our new design, low permeable facer films function as a physical barrier that prevents the diffusion of gases in and out of the foam, thereby minimizing the aging process of the foams over time. In comparison, the foams produced for the study have a higher radiation contribution but significantly lower solid and gas contributions. Because the high-performance foams are anisotropic, the solid and gas contributions cannot be decomposed.[46] They together contribute $k_{solid+gas}$ = 15.2 and 19.4 $mW·m^{-1}·K^{-1}$ before and after aging, respectively, perpendicular to the long side of the cells. These solid and gas contributions are much smaller than those in commercial foams, which are about 20.6 and 24.6 $mW·m^{-1}·K^{-1}$ before and after aging, respectively.

The advancement of the high-performance foams compared with the properties of currently available commercial foams can be attributed to two key factors: (1) the choice of blowing agent and (2) the anisotropic pore structure. Commercial foams typically use pentane as the blowing agent with water as an auxiliary component, which produces CO_2 as a byproduct. Pentane and CO_2 have thermal conductivities of 14.5 and 16.7 $mW·m^{-1}·K^{-1}$ at 24 °C, respectively. In contrast, the high-performance foams utilize hydrofluoroolefin (Opteon 1100) as the blowing agent, which has a lower thermal conductivity of 10.6 $mW·m^{-1}·K^{-1}$ at 24 °C. Additionally, by minimizing the water content in the formulation, the CO_2 concentration is low. Another distinguishing feature is the pore structure of the foam. Although commercial foams have isotropic pores, high-performance foams incorporate anisotropic pores that enhance the thermal insulation. If high-performance foams had isotropic pores instead, their initial R/in. would be less than 6.7, as predicted by ThermoPI models.[56,57] The enhancement by anisotropy of the pores observed in the experiment is consistent with the our finite element simulations.[46]

To gain deeper insights into the thermal conductivity of the high-performance foam with a R/in. of 8.3 and to guide the design of foams with higher R/in. values, we need to extract the thermal conductivity of the gas in the foam, analyze its composition, and explore the lower limit of $k_{solid+gas}$ by adjusting the gas composition and anisotropic ratio. The first step was to determine k_g, the intrinsic thermal conductivity of the gas in the foam with R-8.3/in. Since the radiation thermal conductivity is measured as 2.8 $mW·m^{-1}·K^{-1}$, the $k_{solid+gas}$ can be obtained by $k_{solid+gas} = k_{eff} - k_{rad}$ = 14.5 $mW·m^{-1}·K^{-1}$ (Table 3). With ξ = 3.7 (SEM image analysis), k_s = 0.235 $W·m^{-1}·K^{-1}$ (thermal conductivity of polyurethane),[56] and ϕ = 0.95, k_g can be calculated using the effective medium approximation model developed and validated by Tiwari, Shrestha, and Feng, as shown in eqs 1−3.[46]

$$k_{solid+gas}(\phi, \xi, k_s, k_g) = (1 + x)[xk_s^{-1} + (k_s - \phi(1 + x)(k_s - k_g))^{-1}]^{-1} \quad (1)$$

$$x = \frac{1}{3}\left(a + \frac{(\xi^{1.8} - 1)^2}{a} - 2\xi^{1.8} - 1\right) \quad (2)$$

$$a = \left(\frac{3}{2}\left(12\frac{(\xi^{1.8} - 1)^3\xi^{3.6}}{\phi} + 81\frac{\xi^{7.2}}{\phi^2}\right)^{1/2} + (\xi^{1.8} - 1)^3 + \frac{27}{2}\frac{\xi^{3.6}}{\phi}\right)^{1/3} \quad (3)$$

The results show that k_g = 12.08 $mW·m^{-1}·K^{-1}$, representing the intrinsic thermal conductivity of a gas mixture, is composed of Opteon 1100 (10.7 $mW·m^{-1}·K^{-1}$), CO_2 (16.6 $mW·m^{-1}·K^{-1}$), a byproduct of the foaming process, and air (26.2 $mW·m^{-1}·K^{-1}$) owing to the presence of open pores. The value of k_g is determined by the thermal conductivity of each gas species (k_{g_i}) and its volume fraction f_i from Brokaw[58]

$$k_g = \sum_{i=1}^{n} \frac{f_i}{\sum_{j=1}^{n} f_j A_{ij}} k_{g_i} \quad (4)$$

where n is the total number of gas species. The term A_{ij} is the interaction parameter between gas species i and j, which can be calculated with the Mason−Saxena equation.[59] If no air is

https://doi.org/10.1021/acsaenm.5c00263
ACS Appl. Eng. Mater. 2025, 3, 2087−2098

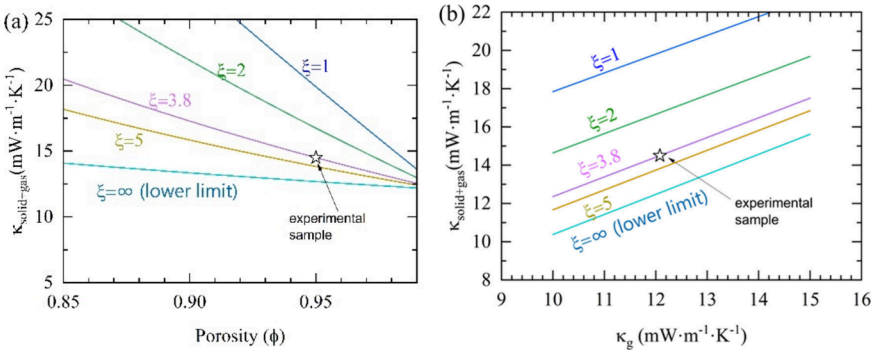

Figure 6. (a) Theoretically predicted $k_{solid+gas}$ (solid and gas contributions to the effective thermal conductivity of the foam) as a function of anisotropic ratio and porosity, and (b) theoretically predicted $k_{solid+gas}$ (solid and gas contributions to the effective thermal conductivity of the foam) as a function of anisotropic ratio and k_g (intrinsic thermal conductivity of the gas in the foam).

present in the foam, the volume fractions of Opteon 1100 and CO_2 are 62% and 38%, respectively. If air is present in the foam, the volume fraction of Opteon 1100 must be greater than 62%.

Anisotropy significantly influences radiative heat transfer by altering the effective pore size along different spatial directions. In anisotropic foams, the pore size is smaller along the direction of heat flow, which reduces the mean free path of thermal photons and thereby suppresses radiative thermal transport. Additionally, such anisotropy concurrently affects gas-phase and solid conduction pathways, often leading to a reduced effective thermal conductivity along the heat transfer direction. Therefore, anisotropy simultaneously reduces the three mechanisms along one direction and increases them in the other directions.

The potential of further reduction of $k_{solid+gas}$ is explored with eq 4. As shown in Figure 6a, if the gas composition and foam porosity remain the same as those in the foam with R/in. of 8.3, increasing the anisotropic ratio can lower $k_{solid+gas}$ to a minimum of 12.5 $mW{\cdot}m^{-1}{\cdot}K^{-1}$. Alternatively, if the anisotropic ratio and gas composition are held constant, increasing the porosity to 97% can reduce $k_{solid+gas}$ to 13.7 $mW{\cdot}m^{-1}{\cdot}K^{-1}$. Likewise, if the anisotropic ratio and porosity remain unchanged, eliminating CO_2 and air while retaining only Opteon 1100 in the foam can lower $k_{solid+gas}$ to 13.2 $mW{\cdot}m^{-1}{\cdot}K^{-1}$ (Figure 6b). The effective medium approximation employed in our work assumes idealized pore geometries (e.g., Voronoi tessellations), uniform pore sizes, homogeneous anisotropy, and fully closed-cell structures. These simplifications enable analytical treatment but may not fully account for complex features such as irregular pore connectivity, open-cell effects, or nonequilibrium gas diffusion, particularly during long-term aging.

4. CONCLUSION

This study introduces high-performance PIR foams with an enhanced initial R-8.3/in., offering 20% improvement over existing commercial PIR foams. This enhancement is attributed mainly to the use of a low-thermal-conductivity blowing agent (hydrofluoroolefin), reduction of water content, incorporation of anisotropic pores, and employment of barrier facers. We clearly identified crucial factors (e.g., moisture, mold design, and pMDI content) that affect the thermal properties of the PIR foams. In the study of the mold effect, the vertical mold improved R/in by 16% compared with that of the horizontal mold, potentially owing to the combined effects of anisotropic pore geometry, higher closed cell content, and blowing agent retention. The results further demonstrate the anisotropic pore geometry, demonstrating a 125% increase in compressive strength of the foams prepared using a vertical mold compared with a horizontal mold. Moreover, the pMDI percentage significantly affected the thermal properties of the PIR foams. The foams prepared with 48% w/w pMDI demonstrated the highest R/in. values compared with those containing 42% and 54% w/w. Because the relationship between pMDI content and R/in. is not linear, additional research is required to fully understand how pMDI content influences both thermal and structural properties of PIR foams. In addition to the higher thermal resistivity of high-performance foams, the TGA experiments show high contents of char formation, suggesting potential higher resistance to fire compared with commercially available PIR foams. Interestingly, the mixtures of blowing agents had an observable effect on the R/in and the density. Furthermore, the addition of a facer film led to a notable 4% increase in the thermal resistivity of PIR foams. This study provides an in-depth analysis of how anisotropic cells influence both thermal and mechanical properties of materials, thus offering valuable insights into their effects on material performance. Ultimately, the study offers practical tools and insights that can be used to improve the R/in. value of PIR foams. The novel high-performance PIR foams with an R-8.3/in., prepared from readily available materials and utilizing simple synthesis methods, greatly enhance both scalability and manufacturability. These characteristics enable large-scale production in industrial manufacturing plants without requiring major modifications in the production line. Consequently, the new formulations can be effectively scaled up to meet commercial demand, promoting broader real-world application while maintaining cost-effectiveness and consistent quality. While the current findings exhibit promising performance and manufacturability, several limitations remain that require further investigation. Continued aging tests are essential for obtaining a thorough understanding of the long-term performance of the novel PIR foams, with and without facer barriers. It is also crucial to evaluate other important factors, including fire performance, dimensional stability, and moisture resistance, as these directly impact the material's reliability in practical applications. Furthermore, investigating alternative materials to isocyanates is a valuable avenue for future research studies. Addressing these considerations in future studies will help optimize the

https://doi.org/10.1021/acsaenm.5c00263
ACS Appl. Eng. Mater. 2025, 3, 2087−2098

formulations for broader commercial acceptance and align them with evolving standards.

AUTHOR INFORMATION

Corresponding Author

Som S Shrestha − *Buildings and Transportation Science Division, Oak Ridge National Laboratory, Oak Ridge, Tennessee 37830, United States;* orcid.org/0000-0001-8399-3797; Email: shresthass@ornl.gov

Authors

Shiwanka V. Wanasinghe − *Buildings and Transportation Science Division, Oak Ridge National Laboratory, Oak Ridge, Tennessee 37830, United States*

Zoriana Demchuk − *Chemical Sciences Division, Oak Ridge National Laboratory, Oak Ridge, Tennessee 37830, United States*

Achutha Tamraparni − *Buildings and Transportation Science Division, Oak Ridge National Laboratory, Oak Ridge, Tennessee 37830, United States*

Janak Tiwari − *Department of Mechanical Engineering, University of Utah, Salt Lake City, Utah 84112, United States*

Tianli Feng − *Department of Mechanical Engineering, University of Utah, Salt Lake City, Utah 84112, United States*

Catalin P. Gainaru − *Chemical Sciences Division, Oak Ridge National Laboratory, Oak Ridge, Tennessee 37830, United States;* orcid.org/0000-0001-8295-6433

Bo Kyung Park − *Buildings and Transportation Science Division, Oak Ridge National Laboratory, Oak Ridge, Tennessee 37830, United States*

Sungjin Kim − *Chemical Sciences Division, Oak Ridge National Laboratory, Oak Ridge, Tennessee 37830, United States;* orcid.org/0000-0002-2068-9189

Diana Hun − *Buildings and Transportation Science Division, Oak Ridge National Laboratory, Oak Ridge, Tennessee 37830, United States*

Tomonori Saito − *Chemical Sciences Division, Oak Ridge National Laboratory, Oak Ridge, Tennessee 37830, United States;* orcid.org/0000-0002-4536-7530

Complete contact information is available at: https://pubs.acs.org/10.1021/acsaenm.5c00263

Notes

This manuscript has been authored by UT-Battelle, LLC, under contract DE-AC05−00OR22725 with the US Department of Energy (DOE). The US government retains and the publisher, by accepting the article for publication, acknowledges that the US government retains a nonexclusive, paid-up, irrevocable, worldwide license to publish or reproduce the published form of this manuscript, or allow others to do so, for US government purposes. DOE will provide public access to these results of federally sponsored research in accordance with the DOE Public Access Plan (http://energy.gov/downloads/doe-public-access-plan).

The authors declare no competing financial interest.

ACKNOWLEDGMENTS

The research described in this paper was sponsored by the U.S. Department of Energy (DOE) Building Technologies Office. We would like to thank DOE for its funding support and chemical companies GAF Materials, BASF, The Chemours Company, Milliken & Company, Stepan Company, and Evonik Industries for providing the samples used in this study. Additionally, we are grateful to the staff at GAF Materials for their valuable guidance and support throughout the research. In addition, we would like to thank Wheatley Steenman for her assistance and support in conducting this research.

REFERENCES

(1) Jelle, B. P.; Gustavsen, A.; Baetens, R. Innovative High Performance Thermal Building Insulation Materials-Todays State-of-the-Art and Beyond Tomorrow. In *Proceedings of the Building Enclosure Science & Technology (BEST 3 - 2012)*; Atlanta, Georgia, April 2-4, 2012.

(2) de Souza, F. M.; Choi, J.; Ingsel, T.; Gupta, R. K. High-Performance Polyurethanes Foams for Automobile Industry. In *Nanotechnology in the Automotive Industry*; Elsevier, 2022; pp 105−129.

(3) Berge, A.; Johansson, P. *Literature Review of High Performance Thermal Insulation*; Chalmers University of Technology: Gothenburg, Sweden, 2012.

(4) Pambudi, N. A.; Sarifudin, A.; Gandidi, I. M.; Romadhon, R. Vaccine Cold Chain Management and Cold Storage Technology to Address the Challenges of Vaccination Programs. *Energy Reports* **2022**, *8*, 955−972.

(5) U.S. Energy Information Administration. *Use of Energy Explained*. 2023. https://www.eia.gov/energyexplained/use-of-energy/homes.php (accessed 08/14/2024).

(6) Al-Homoud, M. S. The Effectiveness of Thermal Insulation in Different Types of Buildings in Hot Climates. *Journal of Thermal Envelope and Building Science* **2004**, *27* (3), 235−247.

(7) Perez-Lombard, L.; Ortiz, J.; Pout, C. A Review on Buildings Energy Consumption Information. *Energy and buildings* **2008**, *40* (3), 394−398.

(8) Hung Anh, L. D.; Pasztory, Z. An Overview of Factors Influencing Thermal Conductivity of Building Insulation Materials. *Journal of Building Engineering* **2021**, *44*, 102604.

(9) Lakatos, A.; Csontos, M.; Csik, A. Investigation of Both Thermal Parameters and Applications of Closed-Cell Plastic Thermal Insulation Foams with Building Energetic Aspects. *J. Therm. Anal. Calorim.* **2024**, *149* (19), 11171−11182.

(10) Ganji, D. D.; Sabzehmeidani, Y.; Sedighiamiri, A. *Nonlinear Systems in Heat Transfer*; Elsevier, 2018.

(11) Paufler, P.; Gibson, L. L.; Ashby, M. F. Cellular Solids. Structure & Properties. Pergamon Press, Oxford 1988. IX+ 357 p. Preis $40.00. ISBN 0−08−036607−4. *Crystal Research and Technology* **1990**, *25* (9), 1038−1038.

(12) Hu, F.; Wu, S.; Sun, Y. Hollow-Structured Materials for Thermal Insulation. *Adv. Mater.* **2019**, *31* (38), 1801001.

(13) Kalnæs, S. E.; Jelle, B. P. Vacuum insulation panel products: A State-of-the-Art Review and Future Research Pathways. *Applied Energy* **2014**, *116*, 355−375.

(14) Forsberg, C. H. *Heat Transfer Principles and Applications*; Academic Press, 2020.

(15) Lakatos, Á.; Lucchi, E. Thermal Performances of Super Insulation Materials (Sims): A Comprehensive Analysis of Characteristics, Heat Transfer Mechanisms, Laboratory Tests, and Experimental Comparisons. *International Communications in Heat and Mass Transfer* **2024**, *152*, 107293.

(16) Lakatos, A.; Kalmar, F. Analysis of Water Sorption and Thermal Conductivity of Expanded Polystyrene Insulation Materials. *Building Services Engineering Research and Technology* **2013**, *34* (4), 407−416.

(17) Vo, C. V.; Bunge, F.; Duffy, J.; Hood, L. Advances in Thermal Insulation of Extruded Polystyrene Foams. *Cellular Polymers* **2011**, *30* (3), 137−156.

(18) Kuhn, J.; Ebert, H.-P.; Arduini-Schuster, M.; Büttner, D.; Fricke, J. Thermal Transport in Polystyrene and Polyurethane Foam

Insulations. *International journal of heat and mass transfer* **1992**, *35* (7), 1795−1801.
(19) Cao, X.; Liu, J.; Cao, X.; Li, Q.; Hu, E.; Fan, F. Study of the Thermal Insulation Properties of the Glass Fiber Board Used for Interior Building Envelope. *Energy and Buildings* **2015**, *107*, 49−58.
(20) Vatin, N.; Pestryakov, I.; Ogidan, T.; Yarunicheva, Y.; Kiryushina, A. Water Vapour by Diffusion and Mineral Wool Thermal Insulation Materials. *Magazine of Civil Engineering* **2018**, *5* (81), 183−192.
(21) Fangueiro, R. *Fibrous and Composite Materials for Civil Engineering Applications*; Elsevier, 2011.
(22) Kymäläinen, H.-R.; Sjöberg, A.-M. Flax and Hemp Fibresas Raw Materials for Thermal Insulations. *Building and environment* **2008**, *43* (7), 1261−1269.
(23) Zach, J.; Korjenic, A.; Petranek, V.; Hroudova, J.; Bednar, T. Performance Evaluation and Research of Alternative Thermal Insulations Based on Sheep Wool. *Energy and Buildings* **2012**, *49*, 246−253.
(24) Ghosh, S.; Singh, S.; Maity, S. Thermal Insulation Behavior of Chemically Treated Jute Fiber Quilt. *Journal of Natural Fibers* **2021**, *18* (4), 568−580.
(25) Baetens, R.; Jelle, B. P.; Thue, J. V.; Tenpierik, M. J.; Grynning, S.; Uvsløkk, S.; Gustavsen, A. Vacuum Insulation Panels for Building Applications: A Review and Beyond. *Energy and Buildings* **2010**, *42* (2), 147−172.
(26) Baetens, R.; Jelle, B. P.; Gustavsen, A. Aerogel Insulation for Building Applications: A State-of-the-Art Review. *Energy and buildings* **2011**, *43* (4), 761−769.
(27) Biswas, K.; Shrestha, S. S.; Bhandari, M. S.; Desjarlais, A. O. Insulation Materials for Commercial Buildings in North America: An Assessment of Lifetime Energy and Environmental Impacts. *Energy and Buildings* **2016**, *112*, 256−269.
(28) Duval, A.; Sarazin, J.; de Haas, C.; Sarbu, A.; Bourbigot, S.; Averous, L. Influence of the Chemical Structure of Polyester Polyols on the Properties and Fire Resistance of Polyisocyanurate Foams. *Eur. Polym. J.* **2024**, *210*, 112938.
(29) Değirmenci, B.; Köken, N.; Akar, A. Smoke Suppressant and Fire-Retardant Polyurethane-Polyisocyanurate (PIR) Foam. *J. Appl. Polym. Sci.* **2023**, *140* (36), No. e54372.
(30) Kalhor, K.; Emaminejad, N. Qualitative and Quantitative Optimization of Thermal Insulation Materials: Insights from the Market and Energy Codes. *Journal of Building Engineering* **2020**, *30*, 101275.
(31) Berardi, U.; Madzarevic, J. Microstructural Analysis and Blowing Agent Concentration in Aged Polyurethane and Polyisocyanurate Foams. *Applied Thermal Engineering* **2020**, *164*, 114440.
(32) Makaveckas, T.; Bliudžius, R.; Burlingis, A. Determination of the Impact of Environmental Temperature on the Thermal Conductivity of Polyisocyanurate (PIR) Foam Products. *Journal of Building Engineering* **2021**, *41*, 102447.
(33) Czuprynski, B.; Paciorek-Sadowska, J.; Liszkowska, J. Modifications of the Rigid Polyurethane-Polyisocyanurate Foams. *J. Appl. Polym. Sci.* **2006**, *100* (3), 2020−2029.
(34) Kuranska, M.; Prociak, A.; Kirpluks, M.; Cabulis, U. Polyurethane-Polyisocyanurate Foams Modified with Hydroxyl Derivatives of Rapeseed Oil. *Industrial Crops and Products* **2015**, *74*, 849−857.
(35) Lazo, M.; Puga, I.; Macias, M. A.; Barragan, A.; Manzano, P.; Rivas, A.; Rigail-Cedeno, A. Mechanical and Thermal Properties of Polyisocyanurate Rigid Foams Reinforced with Agricultural Waste. *Case Studies in Chemical and Environmental Engineering* **2023**, *8*, 100392.
(36) Reignier, J.; Mechin, F.; Sarbu, A. How Increasing Amounts of Trimerization Catalyst Impact the Formation, Isocyanurate Content, and Microstructure of Poly (Urethane-Isocyanurate) Rigid Foams. *Ind. Eng. Chem. Res.* **2024**, *63*, 20824.
(37) Vlasov, R.; Ryabova, D.; Zeynalova, S.; Nazmutdinov, M.; Ryabov, S. Effect of Small Amount of Functionalized Multi-Walled Carbon Nanotubes on the Properties of Rigid Polyisocyanurate and Polyurethane Foam Composites. *Cellular Polymers* **2023**, *42* (3−4), 123−139.
(38) Romero, R. R.; Grigsby, R. A., Jr; Rister, E. L., Jr; Pratt, J. K.; Ridgway, D. A Study of the Reaction Kinetics of Polyisocyanurate Foam Formulations Using Real-Time FTIR. *Journal of cellular plastics* **2005**, *41* (4), 339−359.
(39) Prałat, K.; Ciemnicka, J.; Jankowski, P.; Wierzbicka, E.; Plis, A. Experimental Research on the Thermal Properties of Innovative Insulation Boards Made of Polyurethane-Polyisocyanurate (PUR/PIR). *Polish Journal of Chemical Technology* **2023**, *25* (1), 40−46.
(40) Torres-Regalado, P.; Santiago-Calvo, M.; Gimeno, J.; Rodriguez-Perez, M. A. Thermal Conductivity Aging and Mechanical Properties of Polyisocyanurate (PIR) Foams Produced with Different Contents of HFO. *J. Appl. Polym. Sci.* **2023**, *140* (40), 1−14.
(41) Mukhopadhyaya, P.; Bomberg, M. T.; Kumaran, M. K.; Drouin, M.; Lackey, J.; van Reenen, D.; Normandin, N. Long-Term Thermal Resistance of Polyisocyanurate Foam Insulation with Gas Barrier. In *IX International Conference on Performance of Exterior Envelopes of Whole Buildings, Clearwater Beach, Florida*, 2004; pp 1−10.
(42) Lynch, J.; Moore, M.; Randall, D. A Novel Facer for PIR/PUR Boardstock. *Cellular polymers* **1991**, *10* (2), 117−131.
(43) *Standard Test Method for Steady-State Thermal Transmission Properties By Means of the Heat Flow Meter Apparatus*. 2021. https://www.astm.org/c0518-21.html (accessed 2024 06/03).
(44) International, A. *Standard Test Method for Open Cell Content of Rigid Cellular Plastics*; ASTM International, 2010.
(45) Shieh, D. J. Polyol with high cyclopentane solubility. U.S. Patent US US7560526B2, 2007.
(46) Tiwari, J.; Shrestha, S. S.; Feng, T. Computational Design of Isotropic and Anisotropic Ultralow Thermal Conductivity Polymer Foams. *Journal of Building Engineering* **2024**, *92*, 109717.
(47) Bernardo, V.; Laguna-Gutierrez, E.; Lopez-Gil, A.; Rodriguez-Perez, M. A. Highly Anisotropic Crosslinked HDPE Foams qith a Controlled Anisotropy Ratio: Production and Characterization of the Cellular Structure and Mechanical Properties. *Materials & Design* **2017**, *114*, 83−91.
(48) Wicklein, B.; Kocjan, A.; Salazar-Alvarez, G.; Carosio, F.; Camino, G.; Antonietti, M.; Bergström, L. Thermally Insulating and Fire-Retardant Lightweight Anisotropic Foams Based on Nanocellulose and Graphene Oxide. *Nature Nanotechnol.* **2015**, *10* (3), 277−283.
(49) Lee, T.; Lakes, R. Anisotropic Polyurethane Foam with Poisson'sratio Greater than 1. *J. Mater. Sci.* **1997**, *32*, 2397−2401.
(50) Arora, K. A.; Lesser, A. J.; McCarthy, T. J. Preparation and Characterization of Microcellular Polystyrene Foams Processed in Supercritical Carbon Dioxide. *Macromolecules* **1998**, *31* (14), 4614−4620.
(51) Oliveira-Salmazo, L.; Lopez-Gil, A.; Silva-Bellucci, F.; Job, A. E.; Rodriguez-Perez, M. A. Natural Rubber Foams with Anisotropic Cellular Structures: Mechanical Properties and Modeling. *Industrial Crops and Products* **2016**, *80*, 26−35.
(52) Andersons, J.; Kirpluks, M.; Stiebra, L.; Cabulis, U. Anisotropy of the Stiffness and Strength of Rigid Low-Density Closed-Cell Polyisocyanurate Foams. *Materials & design* **2016**, *92*, 836−845.
(53) Andersons, J.; Cābulis, U.; Stiebra, L.; Kirpļuks, M.; Spārniņš, E. Modeling the Mode I Fracture Toughness of Anisotropic Low-Density Rigid PUR and PIR Foams. *Int. J. Fract.* **2017**, *205*, 111−118.
(54) Gahlen, P.; Stommel, M. Modeling of the Local Anisotropic Mechanical Foam Properties in Polyisocyanurate Metal Panels Using Mesoscale Fem Simulations. *International Journal of Solids and Structures* **2022**, *244*, 111595.
(55) Shrestha, S.; Demchuk, Z.; Polo-Garzon, F.; Tamraparni, A.; Damron, J.; Howard, D.; Saito, T.; Sokolov, A.; Hun, D.; Gainaru, C. An Experimental Toolbox for the Physical Characterization of Thermal Insulating Polymeric Foams. *Heliyon* **2024**, *10* (16), e36074.
(56) Shrestha, S. S.; Tiwari, J.; Rai, A.; Hun, D. E.; Howard, D.; Desjarlais, A. O.; Francoeur, M.; Feng, T. Solid and Gas Thermal Conductivity Models Improvement and Validation in Various Porous

Insulation Materials. *International Journal of Thermal Sciences* **2023**, *187*, 108164.
(57) Feng, T.; Shrestha, S.; Hun, D.; Howard, D.; Rai, A. *ThermoPI Manual*; Buildings and Transportation Science Division, Oak Ridge National Laboratory: Oak Ridge, TN. See the following: https://thermopi.ornl.gov/assets/User_Manual.pdf
(58) Brokaw, R. S. Approximate Formulas for the Viscosity and Thermal Conductivity of Gas Mixtures. II. *J. Chem. Phys.* **1965**, *42* (4), 1140−1146.
(59) Goodman, F. O. Thermal Accommodation Coefficients. *J. Phys. Chem.* **1980**, *84* (12), 1431−1445.

https://doi.org/10.1021/acsaenm.5c00263
ACS Appl. Eng. Mater. 2025, 3, 2087−2098